SYNCHRONOUS GENERATORS CONTROL: FROM THE TRADITIONAL PERSPECTIVE TO THE ICAD FRAMEWORK

Ugalde-Loo, C.E.[*], Vanfretti, L.[‡], Liceaga-Castro, E.[•], Acha, E.[*]

[*] *University of Glasgow, Scotland, UK;* [‡] *Rensselaer Polythechnic Institute, USA;*
[•] *SEPI ESIME IPN Ticoman, México*

Abstract: Automatic voltage regulators and turbine-governors are standard control features in grid-connected synchronous generators. In this paper their performance is evaluated using Individual Channel Analysis and Design. The great benefits of this approach in control system design tasks are elucidated and contrasted to those provided by block diagram representations. Several models of synchronous generators are critically assessed, with reference to a one-machine infinite bus system, and recommendations are made for use in small-signal stability studies. Moreover, careful analysis of the multivariable structure function helps to explain, formally, why some operating conditions of the control system are more critical than others. Two kinds of studies are considered in the paper: one assesses operation under various power factor conditions and the other under a varying tie-line reactance. The performance of conventional controllers is compared with a proposed controller arising from the analysis of the plant dynamical structure.

Keywords: Synchronous Generator, Multivariable Control, Robustness.

1. INTRODUCTION

Heffron-Phillips representations yield invaluable physical insight into the dynamic behaviour of one-machine-infinite-bus (OMIB) systems (Heffron and Phillips, 1952; DeMello and Concordia, 1969). Such models have been extended to include Power System Stabilisers (PSS), sub-transient effects of damper windings and electronically controlled compensation (Larsen, Swann,1981; Saidy and Hughes, 1994; Aree and Acha, 1999). A major asset of the block diagram is that it lends itself to the use of classical and robust control techniques (Rogers, 2000), but eigenanalysis remains industry's preferred approach to assess small signal stability owing to its large-scale applicability (Kundur, 1994), although it may be argued that the approach does not yield physical insight.

On the quest for an analysis tool which does not suffer from lack of physical transparency but which would still be applicable to large-scale systems, a classical oriented framework, termed Individual Channel Analysis and Design (ICAD), has been applied to OMIB systems and other contrived power systems dynamic problems (Fadlalmoula, *et al.*, 1998; Dudgeon, *et al.*, 2000; Edwards, *et al.*, 2000; Ugalde, *et al.*, 2005). ICAD has also been used in induction motor control (Liceaga, *et al.*, 2006).

In this paper the performance of traditional controllers in an OMIB system is assessed using ICAD and the adequacy of several generator order models is critically examined. System performance is studied for different operating conditions and variations in the OMIB's tie-line reactance. ICAD analysis of the dynamical structure of the system is presented and compared with that obtained using block diagrams. Key features of the models and controls being used are highlighted. ICAD, as the control strategy for OMIB systems, has been reported (Fadlalmoula, *et al.*, 1998; Ugalde, *et al.*, 2005), but a critical evaluation of the various models available for analysis is missing in the open literature; such a task is carried out in this paper.

2. BLOCK DIAGRAM MODELLING

The synchronous machine dynamic representation used to derive all models presented in the paper is based on the work of Hammons and Winning (1971).

2.1. Model 1 (5th order model)

The equations (*s*-domain) characterising Model 1 are:

$$\Delta P_e(s) = K_1\Delta\delta(s) + K_2\Delta E_q''(s) - K_{2d}\Delta E_d''(s) \quad (1)$$

$$\Delta E_t(s) = K_5\Delta\delta(s) + K_6\Delta E_q''(s) + K_{6d}\Delta E_d''(s) \quad (2)$$

$$\Delta E_q''(s) = K_3(s)\Delta E_{fd}(s) - K_4(s)\Delta\delta(s) \quad (3)$$

$$\Delta E_d''(s) = K_{4d}(s)\Delta\delta(s) \quad (4)$$

$$\Delta\omega(s) = \frac{1}{2Hs}\left[\Delta P_m(s) - \Delta P_e(s) - D\Delta\omega(s)\right] \quad (5)$$

$$\Delta\delta(s) = \frac{\omega_0}{s}\Delta\omega(s) \quad (6)$$

where the constants and transfer functions are given as in the work of Aree and Acha (1999). Equations (1)–(6) are used to form the block diagram representation for this model, shown in Fig. 1.

2.2. Model 2A (4th order type A model)

Simplifications may be made to reduce modelling complexity and computing overheads while still retaining key generator dynamical effects. The sub-transient effects producing a demagnetising effect due to a change in the rotor by the damping winding may be neglected while still taken into account the transient effects. The following assumptions are made in Model 1: $\tau_{d0}'' \to 0, X_d'' \to X_d', E_q'' \to E_q'$, to yield Model 2A of the synchronous generator. Similarly to Model 1, this is a two-axis generator representation but it considers no damper winding in the *d*-axis. The block diagram representation (not shown) is a particular case of the one given in Fig. 1.

2.3. Model 2B (4th order type B model)

With reference to Model 1, the following simplifying assumptions are made to yield Model 2B:

$$\tau_{q0}'' \to 0, X_q'' \to X_q, E_d'' \to 0$$

This 4th order model is essentially a one-axis model with the field winding and one damping winding in

the *d*-axis. The block diagram representation (not shown) is a particular case of the one given in Fig. 1.

2.4. Model 3 (3rd order model)

This is the classical model presented by DeMello and Concordia (1969), where the dynamical effects of damping windings are all but neglected. This model may be arrived at by making the following assumptions in Model 2A: $\tau''_{q0} \to 0, X''_q \to X_q, E''_d \to 0$.

For quite some time, a debate has existed on what should be the correct generator model to use in order to exact a realistic response of the plant without unduly increasing mathematical complexity. Block diagrams, as a whole, yield physical insight and understanding of the generator's inner behaviour. Equally important is the fact that this representation also enables a transparent analysis of the interaction between input and output variables in terms of constants and transfer functions that encapsulate fully all key dynamic parameters of the system.

3. TRANSFER MATRIX REPRESENTATION

The transfer matrix representation of the various block diagram models can be obtained by suitable manipulation of the relevant equations. Such a representation is desirable and essential for analysis of the synchronous generator plant dynamics under the ICAD framework. The synchronous generator has the following frequency domain representation

$$\begin{bmatrix} \Delta\omega(s) \\ \Delta E_t(s) \end{bmatrix} = \begin{bmatrix} g_{11}(s) & g_{12}(s) \\ g_{21}(s) & g_{22}(s) \end{bmatrix} \begin{bmatrix} \Delta P_m(s) \\ \Delta E_{fd}(s) \end{bmatrix} \tag{7}$$

where $g_{ij}(s)$ are elements of the transfer matrix of the linearised 2*x*2 models of the synchronous generator connected to an infinite bus via a tie-line reactance.

3.1. Model 1

This model is defined by equations (1) to (6). After some arduous algebra the transfer matrix representation of (7) is obtained, where

$$\begin{aligned}
g_{11}(s) &= \frac{(1+\tau''_q s)(Es^2+Fs+G)s}{den(s)}, \qquad g_{12}(s) = -\frac{K_2 A(1+\tau''_{d0}s)(1+\tau''_q s)s}{den(s)} \\
g_{21}(s) &= \omega_0\left[\frac{K_5(Es^2+Fs+G)(1+\tau''_q s) - K_6(B+Cs)(1+\tau''_q s)}{den(s)}\right] + \\
&\quad +\omega_0\left[\frac{K_{6d}C_{4d}(Es^2+Fs+G)}{den(s)}\right] \\
g_{22}(s) &= \frac{A(1+\tau''_{d0}s)}{den(s)}\left\{\left(K_6(1+\tau''_q s)(2Hs+D)s + K_6\left[(1+\tau''_q s)K_1 - K_{2d}C_{4d}\right]\right)\omega_0\right\} + \\
&\quad -\frac{A(1+\tau''_{d0}s)}{den(s)}\left\{\left(K_2\left[(1+\tau''_q s)K_5 + K_{6d}C_{4d}\right]\right)\omega_0\right\}
\end{aligned} \tag{8}$$

given

$$\begin{aligned}
A &= X''_d + X_{tl}, \qquad B = V_{\infty d0}(X_d - X''_d), \qquad E = \tau'_{d0}\tau''_{d0}(X'_d + X_{tl}) \\
C &= V_{\infty d0}\left\{(X'_d - X''_d)\tau'_{d0} + (X_d - X'_d)\tau''_{d0}\right\}, \qquad G = (X_d + X_{tl}) \\
F &= \left[\tau''_{d0}\left\{(X''_d + X_{tl}) + (X_d - X'_d)\right\} + \tau'_{d0}(X'_d + X_{tl})\right] \\
den(s) &= (2Hs+D)(Es^2+Fs+G)(1+\tau''_q s)s + K_1(Es^2+Fs+G)(1+\tau''_q s)\omega_0 + \\
&\quad -K_2(B+Cs)(1+\tau''_q s)\omega_0 - K_{2d}C_{4d}(Es^2+Fs+G)\omega_0
\end{aligned}$$

3.2. Models 2A, 2B and 3

Following a similar line of algebraic manipulation as for Model 1, the corresponding transfer matrix representation is arrived at for the rest of the models.

4. MULTIVARIABLE ANALYSIS

In the framework afforded by ICAD, the dynamical structure of plant (7) is determined by input-output channels resulting from pairing each input to each output by means of diagonal controllers. For instance, the controller $\mathbf{K_1}(s) = diag\left[k_{11}(s), k_{22}(s)\right]$ results in the following channel pairing

$$C_1(s): \Delta P_m(s) \to \Delta\omega(s), C_2(s): \Delta E_{fd}(s) \to \Delta E_t(s)$$

which agrees with that associated to conventional controllers. Coupling between channels is determined by the ICAD parameter $\gamma(s)$, termed Multivariable Structure Function (MSF). Analysis of the MSFs provides an effective basis on which to design controllers and for a transparent and straightforward framework with which to assess the system dynamical characteristics (O'Reilly, Leithead, 1991).

The MSF has an explicit parametrized form which is dependent of the model being used; it is extremely useful in assessing the impact of system parameters changes on system performance (Fadlalmoula, *et al.*, 1998). For instance, for Model 1 the MSF is given by

$$\gamma(s) = \frac{-K_2\left[K_5\Lambda\Gamma - K_6\Gamma(B+Cs) + K_{6d}C_{4d}\Lambda\right]\omega_0}{\Lambda\left\{K_6\Gamma(2Hs+D)s + \left(K_6\left[\Gamma K_1 - K_{2d}C_{4d}\right] - K_2\left[\Gamma K_5 + K_{6d}C_{4d}\right]\right)\omega_0\right\}}$$

where $\Lambda = (Es^2+Fs+G)$ and $\Gamma = (1+\tau''_q s)$.

Two different studies are presented. The first study assesses the behaviour of the plant at different operating conditions (power factors) with a fix value of tie-line reactance. The second one assesses the impact of a varying tie-line reactance and its effect on reactive power requirements.

4.1. Study 1. Operation under different power factors

Three cases of power factor values corresponding to previously studied cases using a block diagram approach (Saidy and Hughes, 1994) are presented. Tie-line reactance has a fixed value of X_t = 0.2 *p.u.*

4.1.1. Case I: Leading Power Factor

The Nyquist/Bode diagrams of the MSFs corresponding to our four models are shown in Fig. 2. As evidenced, Models 2B and 3 do not yield suitable information for analysis, owing to the absence of a damping winding in the *q*-axis. Moreover, the awkward switch-back characteristic, typical in these models (which traduces in an unrealistically exaggerated coupling) yields inadequate phase information in the Bode plots. Therefore, analysis is restricted to Models 1 and 2A.

The existence and design of stabilising compensators $k_{ii}(s)$ can be determined from the characteristics of $\gamma(s)$, revealed by its Nyquist/Bode plots shown in Fig. 2. In this case, it reduces to the existence of controllers $k_{ii}(s)$ which, simultaneously, stabilise both $g_{ii}(s)(1-\gamma(s)h_i(s))$ and $g_{ii}(s)$, with $i,j=1,2$, $i \neq j$.

It should be noticed that a zero mechanical damping term *D* is used as a system parameter in order to assess a more critical condition. Models 1 and 2A offer similar structural characteristics but Model 2A

gives a slightly higher coupling, as shown in Fig. 2. Nevertheless, in absence of static damping the behaviours of Models 2B and 3 are rather different when compared with Models 1 and 2A. This point is shown all the more clear when the switch-back characteristic is looked at in the Nyquist/Bode diagrams, which may reflect poor performance and robustness measures of Models 2B and 3 and not due to a bad control system design.

4.1.2. Case II: Near-unit Power Factor
In this section only Model 1 is analysed. Fig. 3 shows the Nyquist and Bode diagrams of the MSFs. As in Case I, the existence and design of stabilising compensators $k_{ii}(s)$ can be determined from the characteristics of $\gamma(s)$. The analysis for the case of near-unit power factor does not differ significantly from that of leading power factor.

4.1.3. Case III: Lagging Power Factor
The Nyquist and Bode plots of the MSFs associated to Model 1 is shown in Fig. 3. The existence of controllers is determined by the characteristics of the MSFs, reflected by their Bode and Nyquist plots. The analysis carried out for Case I is also applied to the case of lagging power factor.

As a corollary of the previous analysis, it may be stated that independently of the operating points at which the synchronous generator finds itself, the existence of a stabilising controller for channels (considering parings: $\Delta P_m \rightarrow \Delta\omega$ and $\Delta E_{fd} \rightarrow \Delta E_t$) reduces to the existence of controllers $k_{ii}(s)$ which stabilise simultaneously $g_{ii}(s)$ and $g_{ii}(s)(1-\gamma(s)h_i(s))$ with $i,j=1,2$, $i \neq j$. If a multivariable controller is obtained in which the characteristics of the MSFs are addressed correctly, such fixed controller should guarantee stability and robustness for all conditions.

Fig. 3 shows the Nyquist and Bode plots of $\gamma(s)$ of Model 1 for all operating conditions assessed in Study 1. The most critical operating condition occurs when the generator works at lagging power factor. The coupling between channels in this case starts to be considerable. Also, stability robustness decreases as the Nyquist plot moves toward (1,0). Similarly, an increase in active power is associated with a decrease of robustness. Such characteristics are consistent with what is observed in practice.

Notice that the polar plots of $\gamma(s)$ clearly demonstrate that models 2B and 3 contain no damping at the natural oscillation frequency and, as a result, a high switch-back characteristic is present. By addition of the *q*-axis damper in the models, as in Models 1 and 2A, system damping is introduced over the frequency range of concern. It can be concluded that models 2B and 3, including only winding representation in the *d*-axis, do not yield sufficient system damping representation and should be avoided. Models 1 and 2A offer similar structural characteristics to one another; however, Model 1 exhibits a higher level of reliability and accuracy. Whenever computational burden is not an issue, Model 1 should be used.

4.2. Study 2. Different tie-line reactance

A synchronous generator performance assessment is carried out for different values of tie-line reactance. This study is carried out as in the work of Saidy and Hughes (1994), but considering values of tie-line reactance X_{tl} = 0.2, 0.3, 0.4, 0.5 *p.u.* Only Model 1 used. The Nyquist/Bode plots of the associated MSFs for all tie-line reactances are shown in Fig. 4.

As previously discussed, the existence of controllers is determined by the characteristics of the MSFs, reflected by their Bode and Nyquist plots. The analysis for all cases is carried out in a similar manner as the one carried out in Case I of Study 1, since the structural characteristics under varying tie-line reactances are preserved. It should be noticed that the coupling between channels increases with increases in tie-line reactance. Notice that the case of X_{tl} = 0.5 *p.u.* shows some coupling near to 0 *dB* at certain frequencies, as evidenced by the Bode diagram. This is consistent with the fact that for long-distance transmission, with no VARs compensation plant, system operation becomes impaired because of the long electrical distances involved. One other key observation elucidated from the previous analysis is that the larger the amount of reactive power flow in the tie-line reactance (while keeping active power constant), the higher the coupling between channels – and thus becoming more difficult to control the plant.

It is argued by Saidy and Hughes (1994) that the block diagram representation provides a useful basis for the analysis of the generator dynamic performance. However, the frequency response plots of the individual transfer functions offer little information about the structure and characteristics that the controllers should possess in order to have a stable and robust system. In contrast, an appropriate analysis of the MSF gives an effective and complete framework for designing multivariable control systems. In fact, the MSF analysis dictates what characteristics the controllers should have in order to assure stability and robustness. It also provides a measurable quantification of coupling between the input-output channels. Moreover, the MSFs show in a clear and simple manner why some operating conditions are more critical than others.

5. PERFORMANCE ASSESSMENT USING ICAD

Control and stability issues of synchronous machines have received much research attention in the past. In this section, the performance of the conventional controllers is investigated. A simplified exciter with an AVR and a turbine/governor system are used. Unless stated otherwise, Model 1 will be used in the simulations. The following conventional controller

$$\mathbf{K}_1(s) = diag\left[\frac{200}{(s+5)(s+2)}, \frac{6600(s+2.695)}{(s+213.5)(s+0.4208)}\right] \quad (9)$$

is used, whose individual elements are in agreement with the controller structures given by Anderson

(1994) and Saadat (2002). The conventional controller is widely used in academic studies of power systems dynamics; however, it is not difficult to discern that it will incur problems in its operation. Notice that elements $g_{11}(s)$ contain a pure differentiating term. To cope with such feature without drastically changing the expression given in (9), the following controller is suggested

$$\mathbf{K}_2(s) = diag\left[\frac{5285}{s^2(s+5)(s+2)}, \frac{6600(s+2.695)}{(s+213.5)(s+0.4208)}\right] \quad (10)$$

The controller (10) complies with the necessary requirements stated in the analysis of $\gamma(s)$. Also, the performance of the following controller

$$\mathbf{K}_3(s) = diag\left[\frac{900(s+0.5)}{s^2(s+1)^2}, \frac{827(s+3.5)(s+1.5)(s+0.5)}{s(s+10)(s+9)(s+1)}\right] \quad (11)$$

is assessed, obtained after analysing the MSFs.

5.1. Study 1 using conventional controllers

In this study, the control system performance for the OMIB system, at different power factor operations is presented. The speed conventional controller was slightly modified (adding two integrators and tuning the gain). Fig. 5 presents the Bode diagrams of the channels. Stability margins for both channels are acceptable. All step responses present a significant overshoot and none of the unit step responses for the terminal voltage reach the reference (not shown). Nevertheless, the best performance is achieved during leading power factor operation, which is in concordance with the MSF analysis presented previously and with what is observed in practice.

5.2. Study 1 using proposed controllers

Study 1 is carried out under the same conditions as for the other test cases but this time using the proposed controllers. Fig. 6 presents the Bode plots of the channels. It should be remarked that stability margins present an improved result and that the overshoot for all the operating conditions reduces (not shown), in comparison with the performance obtained using conventional controllers. Also, both outputs do reach their unit references –an indication of an improved performance. The best dynamic performance is achieved under leading power factor.

5.3. Study 2 using conventional controllers

Fig. 7 depicts the Bode diagrams of the channels. As the electrical distance increases, an undesirable peak appears in the magnitude of the speed channel after the cut-off frequency. Such phenomenon impacts directly on the system's disturbance rejection capability. At frequencies where the peak presents itself any signal having such frequency values will be amplified; as a consequence, the system is more likely to become unstable. As for the terminal voltage channel, shown in Fig. 7(b), it can be observed that an increase in tie-line reactance reflects in an increase of channel bandwidth. Near to the cut-off frequency values the phase presents undesirable curly trajectories due to the presence of the awkward switch-back characteristic. As the electrical distance increases, this characteristic becomes more pronounced and the phase margins decrease, as shown in the Bode plot of Channel 2.

Similarly, from the step responses (not included) a clear pattern emerges: where the larger electrical distance is, the more oscillatory response will become. As in Study 1, the reference is not reached for the terminal voltage channel.

5.4. Study 2 using proposed controllers

The control system performance at different values of the tie-line reactance is presented in Fig. 8. Similarly to the case when conventional controllers were used, the peak in the Bode plot of Channel 1 is present, with adverse implication on disturbance rejection. The switch-back characteristic is also appearing in Channel 2, with adverse implication on stability performance. Nevertheless, stability margins are improved using controller (11) and Channel 2 reaches its reference. Also, overshoots in the step responses are smaller.

5.5. A note on the models and the controllers

It was concluded that Models 1 and 2A were to be preferred. To further qualify this, Fig. 9 shows the control system performance of all models using conventional controllers (leading power factor). The use of Models 2B or 3 could urge one to think that the control system design was unsatisfactory, while in fact it turns out not to be the case, as evidenced by the performance with Models 1 and 2A. In fact, when performance is evaluated for X_{tl} = 0.5 *p.u.* with Models 3 and 2B, the system turns to be unstable, as shown in Fig. 10(a). In contrast, if Models 1 and 2A are used, the control system is still stable.

The speed conventional controller did not yield a satisfactory response. The controller itself is unable to perform compensation actions. As an example, the Bode diagram for Channel 1 with the system working in leading power factor condition is shown in Fig. 10(b). Due to the poor performance exhibited, an "amended" controller was used in our analysis.

To gain a clear observation of the damping characteristic of the damping windings, a zero mechanical damping term D is used in this paper. Admittedly, physical machines will always contain some mechanical damping and it may be thought that this should be included to be able to make a more meaningful comparison between one-axis and two-axis models. To assess this effect, figure 11 shows the MSF using Model 1 with $D = 0$ and that of Model 3 with $D > 0$. As it can be seen, the only way that Model 3 is able to achieve a "similar" behaviour to that of Model 1 occurs when an exceptionally high value of D is considered.

6. CONCLUSION

In this paper the performance of synchronous generators, AVRs and turbine-governors has been revisited using a control engineering framework,

termed ICAD. ICAD provides an alternative, very insightful framework with which to carry out small-signal stability assessments of OMIB systems. It shows analytical advantages over the physically-oriented block diagram method. The suitable analysis of the MSF is amenable to a complete multivariable control system design. Moreover, the MSF provides a quantification of coupling between input-output channels and a formal explanation as to why some operating conditions are more critical than others.

Two-axis synchronous generator models should be preferred over one-axis models, since the latter have been found to be system damping deficient. One-axis models may lead to inaccurate analysis and a poor control system performance due to the inferior quality of the model used and not to a bad controller in itself. Among the two-axis models, Model 1 should be preferred over Model 2A, owing to its superior reliability and performance.

Simulation results obtained are in agreement with system behaviour observed in practice. It was shown that the most critical operating condition occurs at lagging power factor. Coupling between channels is higher during lagging power factor operation, resulting in a considerable loss of system robustness. It was also noticed that channel coupling increases with electrical distance, decreasing robustness. Similarly, the larger the amount of reactive power that flows from the generating plant to the infinite bus (while keeping active power constant), the higher the coupling between channels is; becoming more difficult to control the plant.

REFERENCES

Aree, P., E. Acha (1999). Block diagram model for fundamental studies of a synchronous generator – static VAR compensator system. *IEE Proc.Gen.,Trans. & Dist.*,**146**, no.5, pp. 507–514.

Anderson, P.M. and A.A. Fouad (1994). *Power system control and stability*. IEEE Press, USA.

DeMello, F.P. and C. Concordia (1969). Concepts of synchronous machine stability as affected by excitation control. *IEEE Trans. Pow. App. & Sys.*, **88**, no. 4, pp. 316–329.

Dudegon, G.J.W., W.E. Leithead, J. O'Reilly and J.R. McDonald (2000). Prospects for the Decentralised Control of Small-Scale Power Networks with Embedded Generation. *IEEE Pow. Eng. Soc. SM*, **2**, no. 2, pp. 1399–1404.

Edwards, F.V., G.J.W. Dudgeon, J.R. McDonald and W.E. Leithead (2000). Dynamics of Distribution Networks with Distributed Generation. *IEEE PES SM*, **2**, no. 2, pp. 1032–7.

Fadlalmoula, Z., S.S. Robertson, J. O'Reilly and W.E. Leithead (1998). Individual channel analysis of the turbogenerator with a PSS. *Int. Journal of Control*, **69**, no.2, pp. 175–202.

Hammons, T.J. and D.J. Winning (1971). Comparisons of synch. – machine models in the study of the transient behaviour of electrical power systems. *IEE Proc.*,**118**,no.10,pp.1442–1458.

Heffron, W.G. and R.A. Phillips (1952). Effects of modern Amplidyne voltage regulator in under excited operation of large turbine generators. *Trans. AIEE*, **71**, pp. 692–697.

Kundur, P (1994). *Power system stability and control*. McGraw-Hill, USA.

Larsen, E.V. and D.A. Swann (1981). Applying power system stabilizers Part I, Part II and Part III. *IEEE Trans. Pow. App. & Sys.*, **100**, no. 6, pp. 3017–3047.

Licéaga, E., C.E. Ugalde-Loo and J. Licéaga (2006). Induction Motor Control by ICAD. Accepted in: UKACC ICC.

Rogers, G (2000). *Power System Oscillations*. Kluwer, USA.

Saadat, H. (2002). *Power System Analysis*. McGraw-Hill, USA.

Saidy, M. and F.M. Hughes (1994). Block diagram transfer function model of a generator including damper windings. *IEE Proc. Gen., Trans. & Dist.*, **141**, no. 6, pp. 599–608.

O'Reilly, J. and W.E. Leithead (1991). Multivariable control by 'ICD'. *Int. Journal of Control*, **54**, no. 1, pp. 1–46.

Ugalde-Loo, C.E., D. Olguin, E. Licéaga and J. Licéaga (2005). Individual Channel Design for Synchronous Generators. *Int. Journal of Emerging Electric Power Systems*, **4**, no. 2, part. 4.

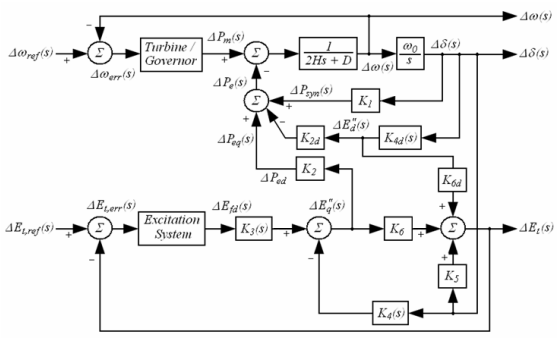

Fig. 1. Block diagram for the OMIB system for Model 1

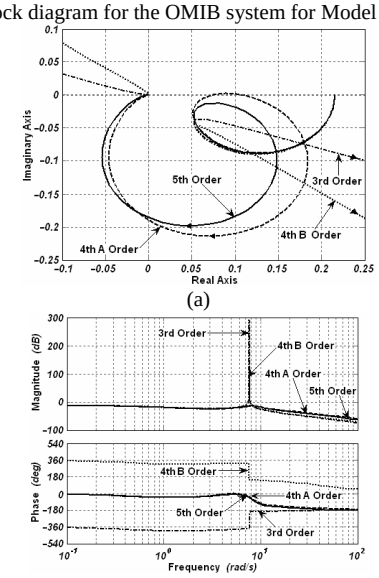

Fig. 2. Assessment of $\gamma(s)$ (Case I). (a) Nyquist and (b) Bode plots

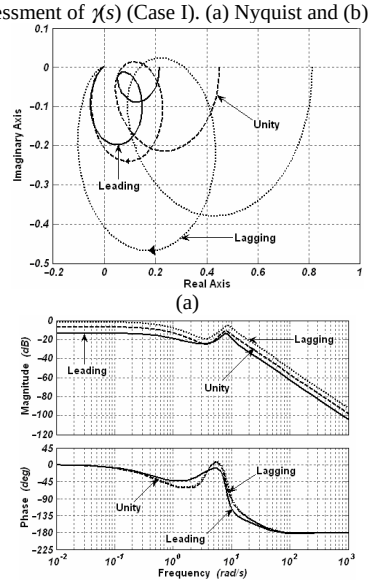

Fig. 3. Assessment of $\gamma(s)$ of Model 1 at three different power factor conditions: (a) Nyquist and (b) Bode plots

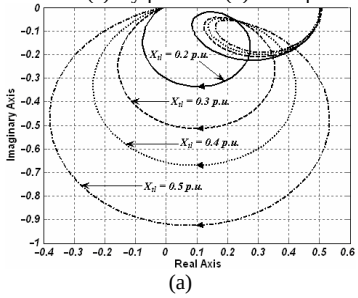

Fig. 4. Assessment of $\gamma(s)$ at different X_{tl}: (a) Nyquist plots

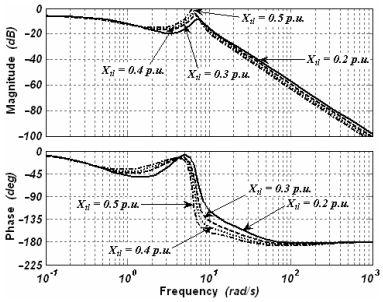

(b)

Fig.4. Assessment of γ(s) at different X_{tl}: (b)Bode plots

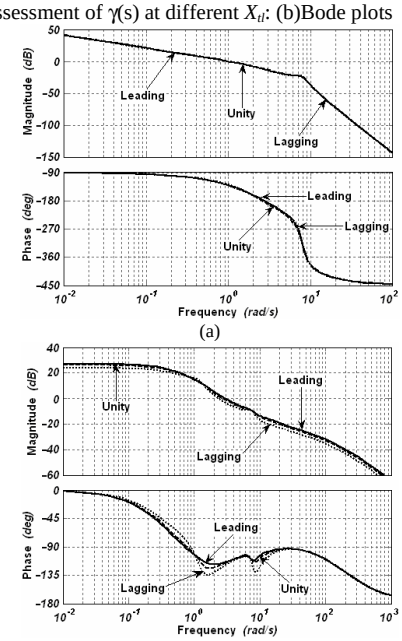

(a)

(b)

Fig.5. Bode plots (conventional controllers): Channel (a) 1; (b) 2

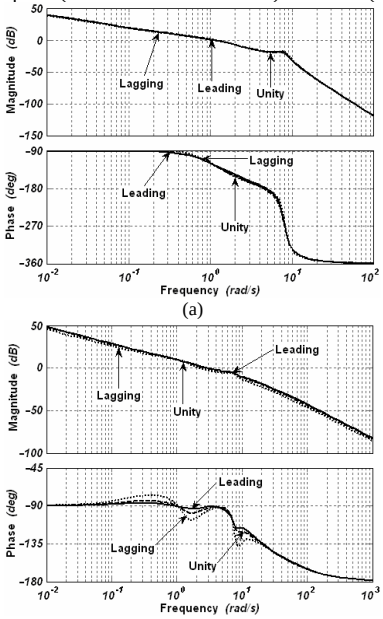

(a)

(b)

Fig. 6. Bode diagrams (designed controllers): Channel (a) 1; (b) 2

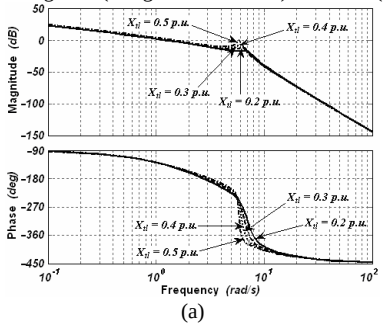

(a)

Fig. 7. Bode plots (conventional controllers): (a) Channel 1

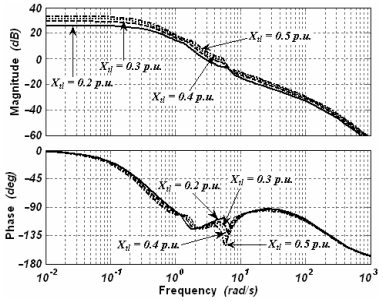

(b)

Fig. 7. Bode plots (conventional controllers): (b) Channel 2

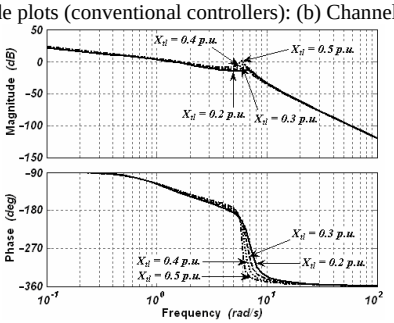

(a)

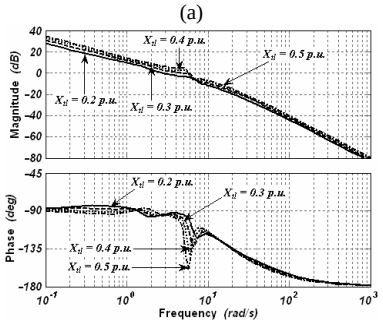

(b)

Fig. 8. Bode diagram (designed controllers): Channel (a) 1; (b) 2

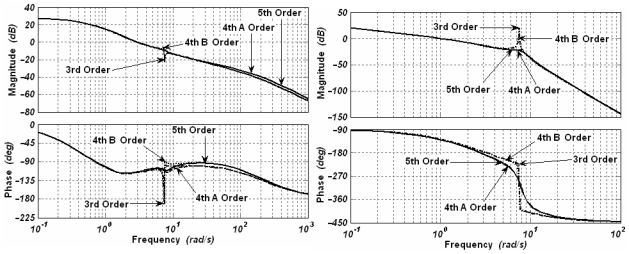

(a) (b)

Fig. 9. Model assessment (leading PF). Bode plot: Ch.l (a) 1; (b) 2

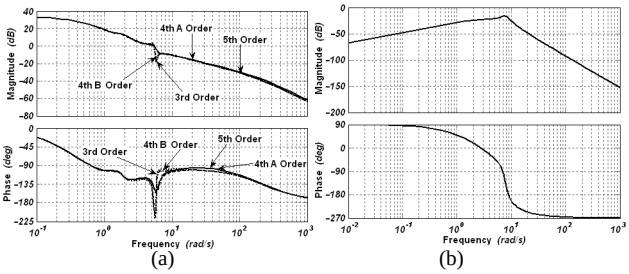

(a) (b)

Fig. 10. (a) Model assessment with X_{tl}=0.5p.u. Ch. 1 Bode plot; (b) Performance of traditional speed controller (leading PF)

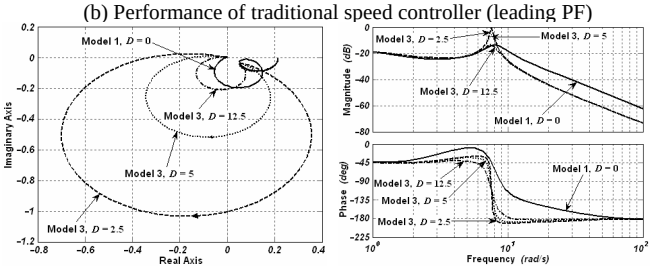

(a) (b)

Figure 11. Assessment of γ(s) at different values of damping term *D*: (a) Nyquist plots; (b) Bode plots.